Final Draft
of the original manuscript:

Laser, T.; Nuernberg, M.; Janz, A.; Hartig, C.; Letzig, D.;
Schmid-Fetzer, R.; Bormann, R.:

The influence of manganese on the microstructure and mechanical properties of AZ31 gravity die cast alloys

In: Acta Materialia (2006) Elsevier

DOI: 10.1016/j.actamat.2006.02.039

The influence of manganese on the microstructure and mechanical properties of AZ31 gravity die cast alloys

T. Laser[a], M. R. Nürnberg[b], A. Janz[c], Ch. Hartig[a], D. Letzig[b], R. Schmid-Fetzer[c], R. Bormann[a]

[a] Hamburg University of Technology, Department of Materials Science and Technology, Eissendorfer Str. 42, D-21073 Hamburg, Germany

[b] GKSS Research Centre, Institute for Materials Research, Max-Planck-Str. 1, D-21502 Geesthacht, Germany

[c] Clausthal University of Technology, Institute of Metallurgy, Robert-Koch-Str. 42, D-38678 Clausthal-Zellerfeld, Germany

Acta Materialia . Vol. 54 (2006) 11, 3033 – 3041

Abstract

Calculated phase diagrams for the Mg-Al-Zn-Mn system indicate that β-Mn(Al) and Al_8Mn_5 can primarily crystallize during the solidification of Mn modified AZ31. Both phases may act as potential heterogeneous nucleants for magnesium grains and thus as potential grain refiners in the Mg-Al system. In this investigation three Mg-3Al-1Zn alloys with different Mn content are die-cast and hot-rolled at 450°C. The influence of the Mn content on the microstructural evolution and mechanical properties after hot-rolling is studied.

After casting, β-Mn and Al_8Mn_5 are present in all three AZ31 alloys without showing significant influence on the grain size. The potential of β-Mn and Al_8Mn_5 precipitates for grain-refinement in AZ alloys is discussed in detail on the basis of solidification kinetics.

Keywords: casting, rolling, magnesium alloys, manganese, grain refinement, solidification modelling

1. Introduction

Magnesium wrought alloys have a great potential for applications in lightweight structural parts. However, their application is still limited due to some undesirable properties: 1) Specific strength and ductility of magnesium alloys are generally inferior to those of common aluminium alloys. 2) Few methods are available for fabricating magnesium products besides casting [1]. In order to overcome these disadvantages, efforts are made to develop wrought magnesium alloys with improved and isotropic mechanical properties. Wrought Mg-3Al-1Zn alloys are of significant interest because they show better strength and increased room-temperature ductility than cast materials due to a more homogeneous microstructure [2]. Furthermore they exhibit a good weldability and a high resistance on corrosion [3]. However, magnesium wrought alloys can only compete against other light weight materials as long as the processing is inexpensive. Therefore, the thermomechanical treatment should preferably start with improved feedstock from cast materials already having small and homogeneous grain sizes. A cast alloy may solidify in a fine grain sized microstructure, if the precipitation of solid particles in the melt or inoculation by extraneous particles is possible. A good example for successful grain refinement is the addition of Zr in non-Al containing Mg alloy [4]. The Mg-Al-Zn system is still a challenge concerning grain refinement. For example, additions of Zr are not suitable due to their immediate reaction with Al in the melt. Thermodynamic modelling indicates however, that with the addition of Mn different kinds of binary Al-Mn phases form during crystallization (compare Fig. 1) and therefore become possible candidates for heterogeneous nucleation sites thus leading to grain refinement. The presence of these second-phase particles can further stimulate the recrystallization kinetics during a thermomechanical treatment, supporting the adjustment of a homogeneous fine-grain-sized microstructure. In order to clarify the potential effect of Mn alloying on the grain refinement during recrystallization, the alloys in this study were hot-rolled and characterized with respect to their evolution of microstructure, texture and some basic plastic properties.

2. Experimental Investigation

The AZ31-based alloys were prepared using pure magnesium (99.95 wt%), pure aluminium (99.95 wt%) and pure zinc (99.8 wt%). Mn was added in form of a master alloy M2 containing Mg with 1.7 wt% Mn. Three different alloys were cast containing 0.28 wt% (I), 0.67 wt% (II) and 0.80 wt% (III) Mn respectively. The AZ31 alloys were melted in a 14-litre steel-made crucible using a resistance furnace. The master alloy M2 and the alloying elements Al and Zn were added to the molten Mg in the crucible at 760°C. Casting was performed under a protective atmosphere of Argon (68.2 l/h) and SF_6 (11.7 l/h). The melt was held at 760°C for 60 min to make sure that the alloying elements were completely dissolved. The alloys were cast into a cylindrical steel container of 10 cm in diameter and 41 cm in length. The weight of the cast billets was about 8 kg. The chemical compositions of the alloys were analysed using the ICPMS Agilent 7500 technique and are shown in Tab. 1. For hot-rolling, blocks with a thickness of 6 mm were cut out of each cast ingot with the rolling direction parallel to the cylindrical axis. All blocks were homogenized at 400°C for 20 h and then air-cooled to room temperature. Before hot-rolling, the blocks were reheated to 450°C for 30 min and then rolled on a two-high mill with a roll diameter of 200 mm. No heating of the mill rolls was applied. Rolling was carried out up to a total strain of $\varphi = 1.6$ achieved over three runs. Each run was followed by subsequent annealing for 30 min at 400°C. In the first run, the samples were rolled three times to a reduction of $\varphi = 0.6$. Between each pass, the specimens were reheated at 450°C for 5 minutes. In the second run, the samples were rolled four times to a total reduction of $\varphi = 0.6$; reheating after each pass was done at 450°C for 3 min. The last run comprised four passes to a total strain of $\varphi = 0.4$. The reheating after each pass was carried out at 450°C for 3 min. Tensile samples parallel (RD) and perpendicular (TD) to the rolling direction were machined out of the resulting sheet material (sheet dimensions: ~1,2 mm x 200 mm x 300 mm). Room temperature tensile tests were performed on a Zwick universal testing machine at a constant strain rate of $1 \cdot 10^{-4}\ s^{-1}$. All specimens for optical microscopy were sectioned, cold-mounted, polished and then etched in a solution of picric and acetic acid [5]. Microstructures were observed by optical (LEICA DMLM) and scanning electron microscopy (ZEISS DSM 962) using an accelerating voltage of 20 keV. The grain sizes of the as-cast condition were measured at the outer surface, in the centre of transverse sections and in between (D/4) using the linear intercept method [6] in accordance with ASTM E 112-96.

The textures of the rolled sheets were measured on a D8 DISCOVER X-ray diffractometer (BRUKER AXS Inc.) using reflection geometry and Cu-K_α radiation. The orientation distribution function (ODF) and complete pole figures were calculated using the harmonic method of Bunge [7].

3. Thermodynamic Calculations

A phase diagram section for the alloy series Mg-3.1Al-1Zn + Mn was calculated using the database of Ohno et al. [8] and is presented in Fig. 1. In addition, metastable extrapolations for liquidus lines of β-Mn and Al_8Mn_5 as well as the positions of the three alloys investigated in this study are included. As shown in Fig. 1, in equilibrium state different primary phases are expected to form depending on the Mn content of the alloy: (Mg) for alloys < 0.32 wt% Mn, β-Mn for alloys > 0.53 wt% Mn and Al_8Mn_5 for alloys in between. β-Mn will transform to Al_8Mn_5 below ~660°C. The precipitation of (Mg) at 630°C and the solidus line at 550°C are nearly independent of the temperature regarding the alloy compositions investigated in this paper. However, one cannot expect to achieve thermodynamic equilibrium with the cooling rates applied in normal casting conditions. Therefore, kinetic models for faster solidification have to be taken into consideration to obtain additional information on the non-equilibrium states. We chose the Scheil-Model for our solidification-calculations and utilize the same thermodynamic database as applied to calculate the equilibrium phase diagram (Fig. 1). In the Scheil-Model it is essentially assumed that no diffusion occurs in solid state, but local equilibrium is achieved at the liquid/solid interface [9]. Furthermore, the phase amounts of the individual phases are of central relevance.

Therefore, the presentation of phase amount vs. temperature has proven to be the best way to illustrate a solidification process. The results for the three experimentally investigated AZ31 alloys are given in Fig. 2a-c. The legend also represents the order of appearance of the solid phases. According to the calculations, solidification of (Mg) is limited to a narrow temperature range for all alloys, and only for alloy I, (Mg) will precipitate as primary phase. Based on the calculations, we can expect a very small amount of β-Mn in alloy II, as most of the added Mn is precipitated in form of Al_8Mn_5. Alloy III is predicted to primarily precipitate a larger β-Mn amount of about 0.2 at% before nucleating Al_8Mn_5. It is interesting to note that both alloys II and III will form a very similar amount of Al_8Mn_5 as second phase, indicating that primarily formed β-Mn is not transformed to Al_8Mn_5 under our model assumptions.

4. Experimental Results

4.1 Microstructures after casting

Figs. 3a-c show the macrographs of the cast ingots of Mg-Al-Zn-Mn. For all three alloys with different amounts of Mn (0.28 wt% I, 0.67 wt% II and 0.80 wt% III) the figures show an equiaxed microstructure. As can be seen in Fig. 4, increasing the Mn content from 0.28 wt% up to 0.80 wt% does not produce any significant refinement of the grain size under our experimental conditions. As mentioned in the experimental procedure, the grain size was measured in three different regions of the sample. There are no significant variations in grain size from the centre to the edge of the casting as a result of different cooling rates. The mean grain sizes of alloys I, II and III in as-cast condition at the outer surface, D/4 and the central region of the transverse section are shown in Fig. 4 and are within the range of 350 µm to 450 µm. The micrographs in Figs. 5a-c show the distribution of second phase particles. All figures exhibit dark spots that developed during the etching of the γ-phase $Mg_{17}Al_{12}$. A closer look into the microstructures reveals the existence of smaller second-phase particles, which are different from γ-$Mg_{17}Al_{12}$. Figures 6a-d show the microstructures of alloys I-III using SEM. Analysis of the second phase particles by energy dispersive spectroscopy (EDS) indicates a Mn content between 65 wt% and 87 wt% (rest Al) in all these alloys. Considering the binary phase diagram of Al-Mn [8], a manganese content between 50 wt% and 69 wt% corresponds to Al_8Mn_5 and a manganese content above 75 wt% to β-Mn. About eight particles of each alloy were analysed in detail. From these results, the rhombohedral shaped particles 2, 4 and 6 in Fig. 6 were determined to be Al_8Mn_5 with a manganese content from 65 to 66 wt%, whereas the cubic particles 1, 3 and 5 with a manganese content between 77% and 87 wt% were detected to be β-Mn.

4.2 Microstructures of hot-rolled sheets

Hot-rolling of sheets resulted in fine-grained and equiaxed microstructures which are presented in Fig. 7. Deformation twins were not observed in all examined sheets. Second phase particles of Al-Mn are distributed preferably at grain boundaries, but also found in the interior of the grains. In addition, the rolling process produces a fragmentation of some second phase particles (Fig. 7d). By EDS analysis a maximum of 74 wt% Mn was found in the fragmented particles, whereas the unsplit particles contain at least 78 wt% Mn, indicating that preferably Al_8Mn_5 particles were

fragmented. The mean grain sizes of the rolled sheets are presented in Tab. 2. The two lower manganese concentrations exhibit a grain size approximately 10 % larger than the 0.80 wt% Mn AZ31 sheet. But taking into account the relatively large scatter of grain sizes of each alloy, this difference is insignificant. In Fig. 8, the (0002) (basal) pole figures of the sheets are presented. All alloy modifications show a basal fibre texture which says that most of the grains have their caxis perpendicular to the rolling plane. This texture is commonly observed for multipass rolling with annealing between two passes [10]. The texture for the 0.28 wt% Mn AZ31 exhibits a maximum intensity of 9.15 and is slightly more pronounced than the textures of the higher Mn modified AZ31 sheets, which are almost equal.

4.3 Mechanical properties

The mechanical properties of the tested tensile specimens are shown in Tab. 3. In rolling direction, only the 0.80 wt% Mn modification shows a 5 % higher yield strength. In transverse direction all sheets exhibit approximately the same yield strength. As a consequence, alloy III has a distinctly lower anisotropy of yield stresses ($YS_{TD}/YS_{RD} = 1.02$) than alloys I and II ($YS_{TD}/YS_{RD} = 1.09$). The ultimate tensile strength does not show a difference for the 0.80 wt% Mn modification. All values in rolling direction are in good accordance. In transverse direction the ultimate tensile strength is somewhat lower for the 0.28 wt% Mn AZ31 modification (note however that the scattering is rather large in this case). This material also shows the shortest elongation to failure. Summarizing the results of the tensile tests, the rolling direction exhibits higher elongation to failure and lower strength, whereas in transverse direction, the flow strength is distinctly higher at lower values of elongation to failure. The multi-pass rolling process produces small but distinct differences in the mechanical properties in rolling and transverse direction.

5. Discussion and Conclusions

The Mg-Al-Zn-Mn phase diagram indicates that the alloys containing 0.67 and 0.80 wt% Mn solidify over a different pathway than the alloy containing 0.28 wt% Mn (Fig. 1): with the addition of 0.28 wt% Mn, (Mg) is the primarily nucleating phase. However, for alloys containing 0.67 and 0.80 wt% Mn, β-Mn is primarily precipitated followed by the formation of Al_8Mn_5 before nucleating (Mg). Thus grain refinement through inoculation caused by β-Mn and / or Al_8Mn_5 particles may be possible in these AZ31 alloys. In the present investigation, β-Mn particles as well as Al_8Mn_5 particles could be identified in all three alloys investigated.Yet under the casting conditions used in this study, they do not have an obvious influence on the mean grain size of the alloys in the solidified state. In other investigations, grain refinement by manganese additions in Mgalloys has been reported [11, 12]. However in Ref. 11, the inoculation resulted from the presence of the metastable hexagonal ε-AlMn phase, which was added to the melt. This phase cannot form in our alloys due to thermodynamic constraints. Precipitates of β-Mn in the final casting state seem to be in conflict with the Mg-rich part of the phase diagram for the Mg-Al-Zn-Mn system given in Fig. 1. According to the phase diagram, in alloy I (Mg) and Al_8Mn_5 could be formed simultaneously as first phases during solidification (the very narrow range of primary (Mg) may be disregarded) whereas in alloys II and III, β-Mn particles should first be precipitated, which will be consumed at ~660°C to form Al_8Mn_5. Below 400°C Al_8Mn_5 should transform to $Al_{11}Mn_4$.

As pointed out in chapter 3, one cannot expect to achieve equilibrium in normal casting conditions. Therefore, we have to take models for faster solidification into consideration (Scheil-model) for a reasonable interpretation of the micrographs. The curves in Fig. 2a-c show the results of a calculation of solidification using the Scheil model. Let us first consider alloy III: based on Fig. 2c, the Scheil model predicts β-Mn-particles as primary phase and Al_8Mn_5-particles as secondary phase. Consistently, these phases are also observed by microscopic characterization. Secondly, Fig. 2b shows that alloy II will initially form a very small amount of β-Mn which is followed by Al_8Mn_5 precipitation. This prediction is also in qualitative agreement with the microstructural observation. Thirdly, for alloy I two scenarios are possible: either the Al_8Mn_5 precipitates as primary phase due to supercooling of the melt by ~13.5 K, which is indicated in Fig. 1 with the dashed line extension of the Al_8Mn_5 liquidus line, followed by a huge boost of (Mg)-solidification. Alternatively, Al_8Mn_5 particles are not primarily precipitated but form during

co-solidification of (Mg) and Al_8Mn_5, which occurs just 4 K below the equilibrium liquidus of 630°C. The latter seems to be more likely, as a supercooling > 10 K is usually not observed under our experimental conditions. However, the observation of β-Mn particles in alloy I by SEM (c.f. chapter 4.1) cannot be explained by the phase diagram and the kinetic calculations presented here. Therefore, we propose that the precipitation of β-Mn may originate from a local imbalance of Mn composition in the melt, or by a high nucleation barrier of Al_8Mn_5 (see below). Thus the kinetic modelling indicates that at least in alloys II and III inoculant particles of two phases (β-Mn and Al_8Mn_5) exist in the melt. These particles are possible sites for heterogeneous nucleation of (Mg). Solidification by inoculation with such particles can be accomplished if the cooling rate is high enough for a sufficient nucleation rate of these particles. A necessary condition for a high nucleation rate is a low kinetic barrier, which in this case means low interfacial energy of β-Mn- and Al_8Mn_5-particles in the melt. On the other hand, the cooling rate should be low enough to allow a suitable growth of the primary particles. Further, in order that these particles act as heterogeneous nucleation sites, the interfacial energy of the primary nucleated particles with respect to the solid magnesium has to be low. Considering the results of the kinetic modelling, the shape of β-Mn particles (Fig. 6) indicates that they are primarily nucleated and grown to a µm-range size. Therefore, nucleation of β-Mn phase is possible under our experimental conditions. Based on the kinetic calculations (Fig. 2), the molar fraction of β-Mn amounts to about 0.1 at.% and 0.2 at% for alloys II and III respectively. These values should be considered as upper bounds for the molar fraction of heterogeneous nucleation sites. An estimate of volume fraction based on our SEM analysis gives a value of about 0.03 vol% for β-Mn and a particle density of about 10^{12} particles/m^3. As only those particles were counted, whose compositions were clearly determined, this fraction corresponds to a lower limit. Together with the other microscopic investigations, these results indicate reasonable ranges for the volume fraction, the particle density and the particle sizes to achieve potential grain refinement well below the observed 400 µm size. We therefore conclude that the formed β-Mn phase is not very effective as heterogeneous nucleation sites, due to the relatively high interfacial energy with respect to (Mg). In fact, β-Mn has a rather high atomic mismatch energy against crystalline magnesium compared to other successful inoculants in Mg-Al, when close-packed planes are considered [13]. The evaluation of the grain refinement potential of Al_8Mn_5 is not that straightforward. First, despite the fact that the kinetic modelling indicates that Al_8Mn_5 may nucleate primarily, the Scheil model does not consider nucleation barriers for precipitation. However, nucleation barriers for complex

intermetallic compounds can be substantial, due to large interfacial energies. This would result in a shift of the formation temperature and, consequently, a much smaller volume fraction of Al_8Mn_5 precipitated before nucleating the (Mg) than predicted by Fig. 2b and 2c. Depending on the processing conditions, it may even result in a situation where Al_8Mn_5 is not at all precipitated prior to the formation of (Mg), due to the small temperature difference between the formation of both phases. Secondly, the shape of the Al_8Mn_5 particles does not unambiguously indicate their formation in the melt. Therefore, as primary precipitation of Al_8Mn_5 particles cannot be confirmed clearly in our investigation, their general grain refinement potential for Al-containing Mg alloys remains open. Yet Al_8Mn_5 particles may occur as primary precipitates in Magnesium alloys with higher Aluminium content. Indications of a grain refinement by Al_8Mn_5 in such a case have been reported [12]. Nevertheless, with respect to AZ31 alloys, our results indicate that significant grain refinement by Al_8Mn_5 particles is not observed under our experimental conditions. This can originate from the constraints of Al_8Mn_5 nucleation mentioned above, but also from a high interfacial energy with respect to (Mg). Structural considerations show that similar to β-Mn, Al_8Mn_5 also has a rather high atomic mismatch energy against the hcp (Mg) when close-packed planes are considered, thus limiting its effectiveness as a heterogeneous nucleation site [14]. An improvement of grain refinement during recrystallization caused by Mn additions was not found either: an influence on recrystallization from any particles (Al_8Mn_5 or β-Mn) cannot be stated, as can be seen from the micrographs of the hot-rolled sheets (Fig. 7). This may be related to the small volume fraction of Al_8Mn_5 and β-Mn particles. Most of the mechanical properties (yield stress in transverse direction, tensile strength, strain to fracture) after the thermomechanical treatment do not show a distinct dependence on chemical composition. The anisotropy of yield strengths observed in this work are typical for well annealed AZ31 sheets [10]. However, the small change of the yield stress in the rolling direction and of the plastic anisotropy between alloy II and alloy III remains difficult to understand: it cannot be explained by the difference in texture, which is more significant for alloys I and II (where the anisotropy in strength is equal) than for alloys II and III. Thus this effect must be due to peculiarities of the microstructure, such as the arrangement and density of dislocations or the local correlation of grain orientations. The higher addition of 0.1 wt% Mn may influence the kinetics of recovery or the mobility of grain boundaries resulting in these microstructural effects. A further study of this topic requires more intricate experimental work and is beyond the scope of the present investigation.

Acknowledgements

The authors would like to thank Prof. K. U. Kainer, GKSS Forschungszentrum, Institute for Materials Research, for stimulating discussion. This study was supported by the German Research Foundation (DFG) in the Priority Program SPP Nr. 1168 “InnoMagTec”.

References

[1] Neite G, Kubota K, Higashi K, Hehmann F. Magnesium-Based Alloys. In: Cahn RW, Haasen P, Kramer EJ, editors. Materials Science and Technology: A Comprehensive Treatment, vol. 8. Weinheim: Wiley-VCH, 1996. p.113.

[2] Stalmann A, Sebastian W, Friedrich H, Schumann S, Droder K. Properties and processing of magnesium wrought products for automotive applications. Adv Eng Mater 2001;3:969.

[3] Avedesian MM, ASM International. Handbook Committee. Magnesium and magnesium alloys. Materials Park, OH: ASM International, 1999.

[4] StJohn DH, Qian M, Easton MA, Cao P, Hildebrand Z. Metall Mater Trans A 2005;36A:1669.

[5] Kree V, Bohlen J, Letzig D, Kainer KU. Praktische Metallographie 2004;41:233.

[6] Exner HE, Hougardy HP. Einführung in die quantitative Gefügeanalyse. Oberursel: Dt. Ges. für Metallkunde, 1986.

[7] Bunge H-J. Texture analysis in materials science: mathematical methods. Göttingen: Cuvillier, 1993.

[8] Ohno M, Schmid-Fetzer R. Z Metallkd 2005;96:857.

[9] Scheil E. Z Metallkd 1942;34:70.

[10] Agnew SR. In: Kaplan HIE, editor. TMS annual meeting: TMS The Minerals Metals & Materials Society, 2002. p.169.

[11] Cao P, StJohn DH, Qian M. In: Ke W, Han EH, Han YF, Kainer KU, Luo AA, editors. International Conference on Magnesium Science, Technology and Applications. Beijing: Trans Tech Publications, 2005. p.139.

[12] Byun J-Y, Kwon SI, Ha HP, Yoon J-K. In: Kainer KU, editor. International Conference on Magnesium Alloys and their Applications. Wolfsburg: Wiley-VCH, 2003. p.713.

[13] Guenther R. unpublished. Hamburg University of Technology, 2005.

[14] Zhang MX, Kelly PM, Qian M, Taylor JA. Acta mater 2005;53:3261.

Alloy	Composition, wt%									
	Mg	Al	Zn	**Mn**	Ca	Si	Fe	Ni	Cu	Others
I	Balance	3.1	1.0	**0.28**	<0.01	<0.01	0.006	<0.001	<0.001	<0.1
II	Balance	3.05	1.3	**0.67**	0.015	0.01	0.011	<0.001	<0.001	<0.1
III	Balance	3.05	1.25	**0.80**	0.015	0.01	<0.005	<0.001	0.003	<0.1

Tab. 1. Chemical compositions of the studied alloys

Alloy		Mean grain size / µm	Standard deviation / µm
I	AZ31 with 0.28 wt% Mn	14.0	8.3
II	AZ31 with 0.67 wt% Mn	14.1	8.0
III	AZ31 with 0.80 wt% Mn	12.8	7.1

Tab. 2. Grain sizes of hot-rolled sheets, Gaussian standard deviations calculated from 800 grains

Alloy		YS / MPa		UTS / MPa		% Elong.	
		RD	TD	RD	TD	RD	TD
I	AZ31 with 0.28 wt% Mn	150 ± 1	163 ± 1	249 ± 2	233 ± 12	21 ± 6	6 ± 2
II	AZ31 with 0.67 wt% Mn	148 ± 2	161 ± 1	245 ± 13	256 ± 1	14 ± 6	16 ± 2
III	AZ31 with 0.80 wt% Mn	158 ± 1	161 ± 1	249 ± 7	250 ± 2	22 ± 7	9 ± 4

Tab. 3. Mechanical properties of hot-rolled sheets, errors are Gaussian standard deviations from 3-5 test specimens

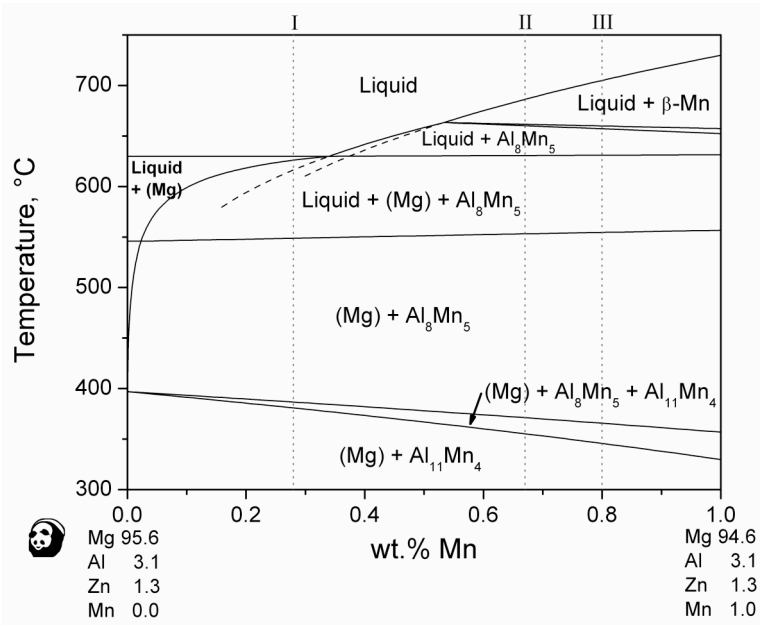

Fig. 1. The Mg-rich part of the phase diagram of the Mg-Al-Zn-Mn system. Dashed line shows metastable extrapolation L/L+β-Mn and L/L+Al_8Mn_5. Dotted lines show alloys I, II and III.

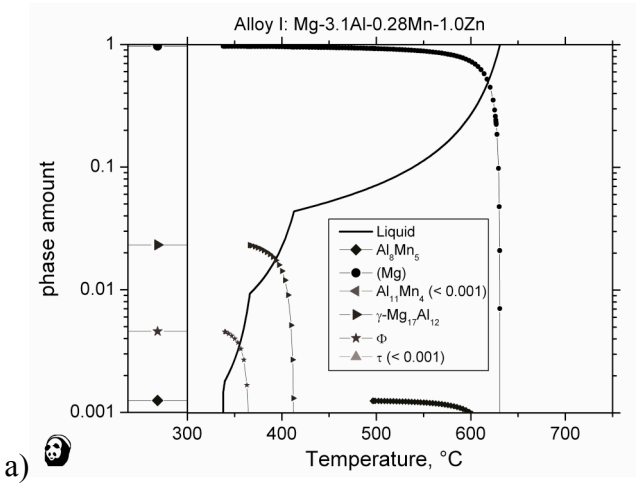

a)

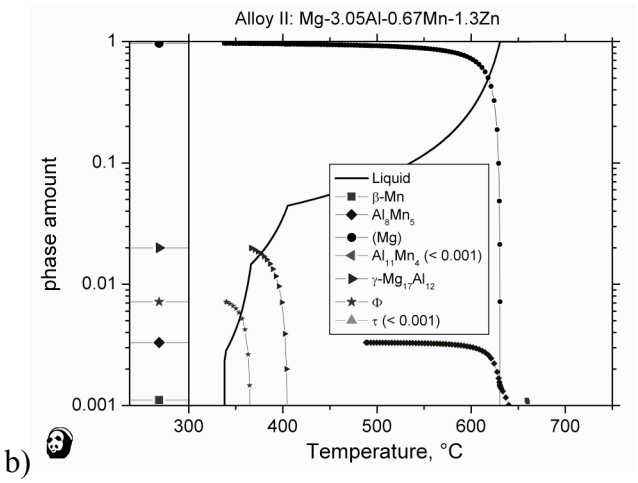

b)

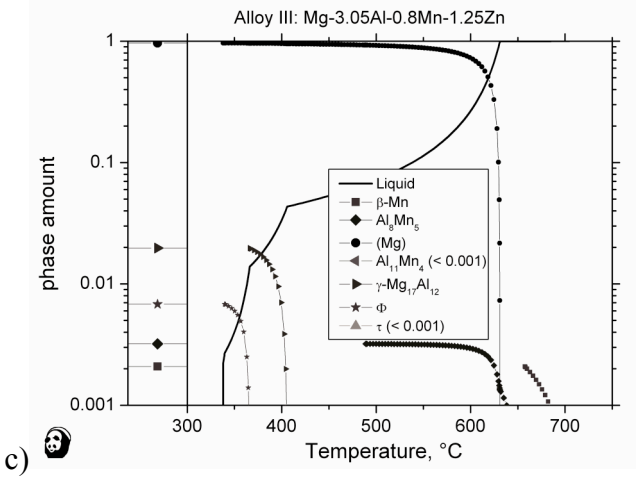

c)

Fig. 2. Phase amount (atomic fractions) calculated for rapid solidification under Scheil conditions vs. temperature for AZ31 with (a) 0.28 wt% Mn alloy I, (b) 0.67 wt% Mn alloy

II and (c) 0.80 wt% Mn alloy III. The final amount of frozen-in solid phases is indicated in the box at the left side of the diagram.

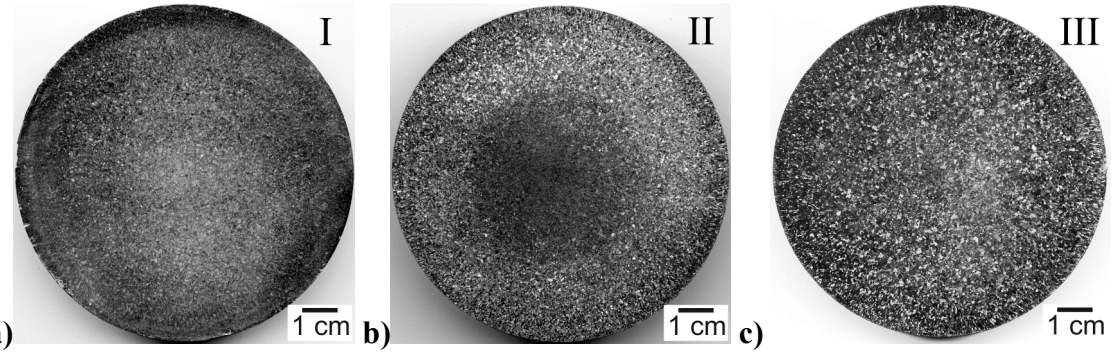

Fig. 3. Macrographs (transversal section) of as cast AZ31 with (a) 0.28 wt% Mn alloy I, (b) 0.67 wt% Mn alloy II and (c) 0.80 wt% Mn alloy III

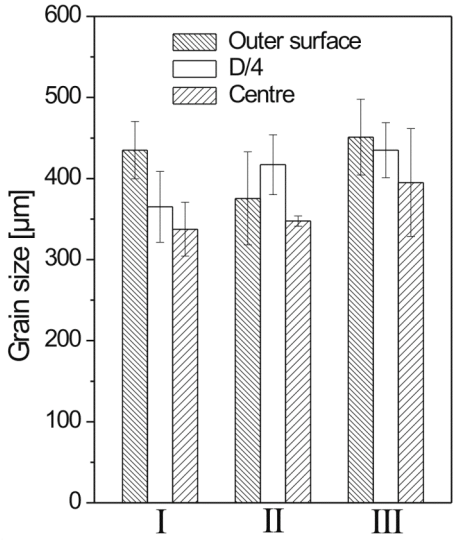

Fig. 4. Mean grain size at outer surface, mid-radius (D/4) and central region of the different alloys I, II and III. Error bars indicate the scatter of mean grain sizes in different fields.

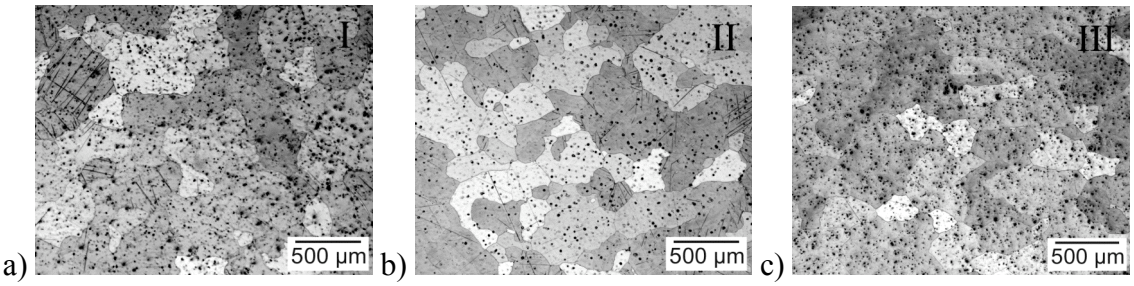

Fig. 5. Microstructure (transversal section) of AZ31 with (a) 0.28 wt% Mn alloy I, (b) 0.67 wt% Mn alloy II and (c) 0.80 wt% Mn alloy III

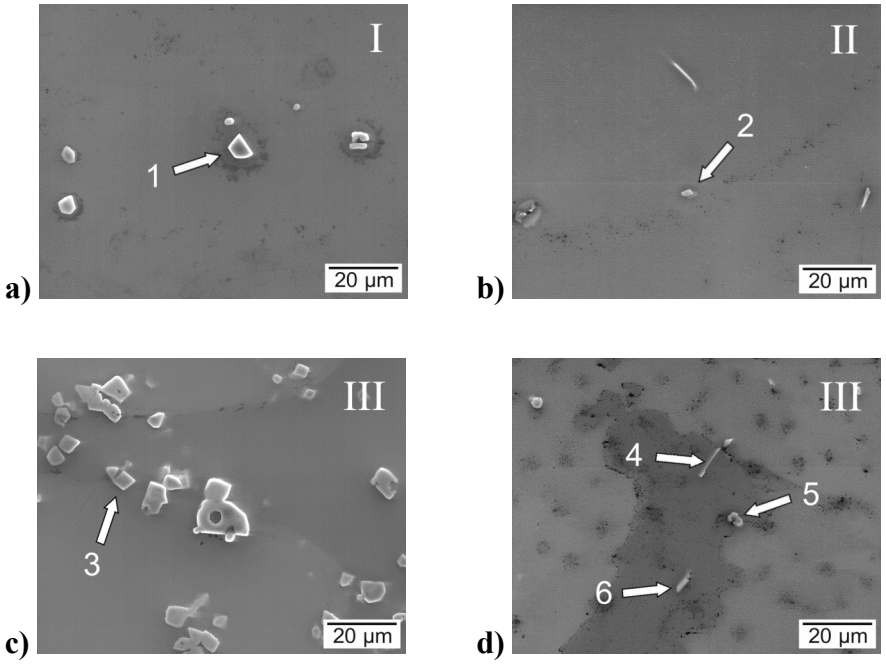

Fig. 6. SEM images (transversal section) of AZ31 with (a) 0.28 wt% Mn alloy I in as-cast condition, (b) 0.67 wt% Mn alloy II in as-cast condition and (c) 0.80 wt% Mn alloy III in as-cast condition and (d) 0.80 wt% Mn alloy III heat treated for 20h at 400°C. Particles 1,3 and 5 are identified as ß-Mn, 2, 4 and 6 as Al_8Mn_5.

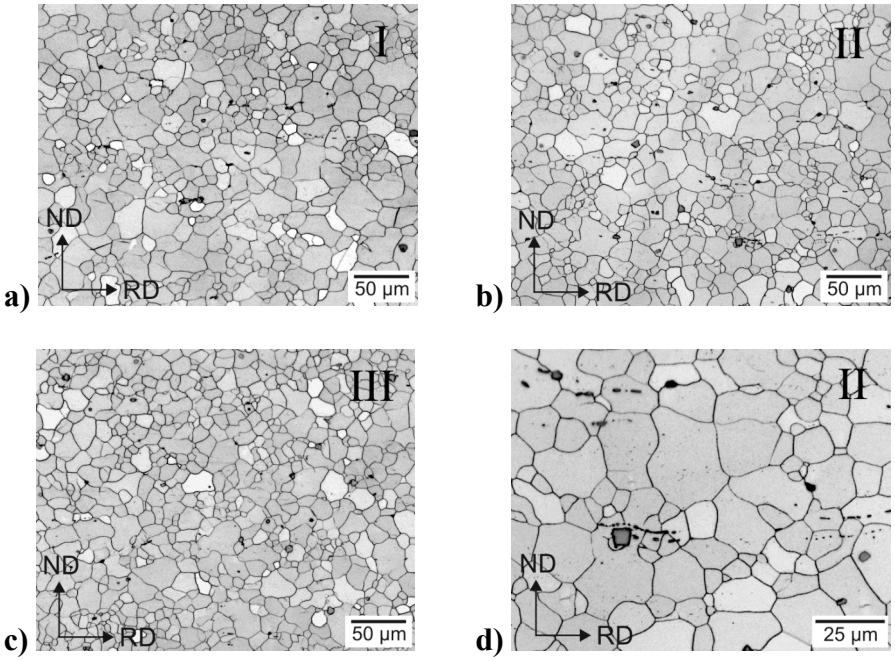

Fig. 7. Microstructures after hot-rolling of AZ31 with (a) 0.28 wt% Mn alloy I, (b) 0.67 wt% Mn alloy II, (c) 0.80 wt% Mn alloy III and (d) detail of b)

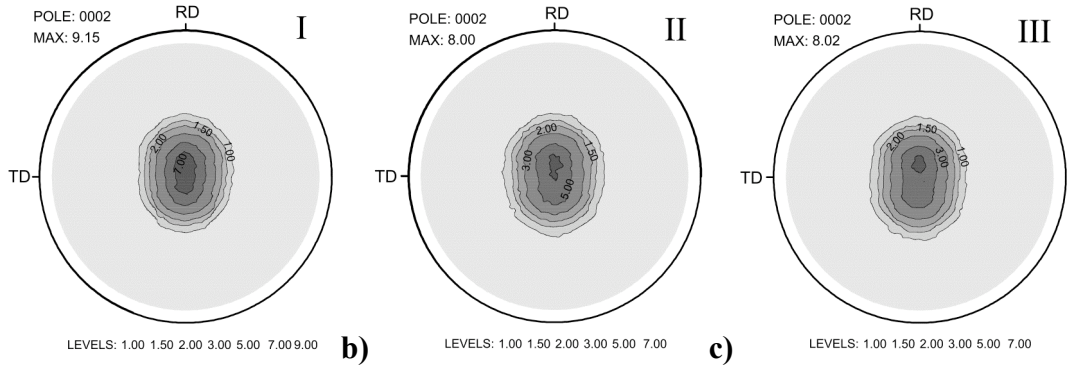

Fig. 8. (0002) pole figures of hot-rolled AZ31 sheets with (a) 0.28 wt% Mn alloy I, (b) 0.67 wt% Mn alloy II and (c) 0.80 wt% Mn alloy III